Cellular/Molecular

Bestrophin-1 Encodes for the Ca^{2+}-Activated Anion Channel in Hippocampal Astrocytes

Hyungju Park,[1]* Soo-Jin Oh,[1]* Kyung-Seok Han,[1,4] Dong Ho Woo,[1,4] Hyekyung Park,[1] Guido Mannaioni,[2] Stephen F. Traynelis,[3] and C. Justin Lee[1,4]

[1]Center for Neural Science, Convergence Technology Laboratory, Korea Institute of Science and Technology, Seoul 136-791, Korea, [2]Department of Pharmacology, University of Florence, 50121 Florence, Italy, [3]Department of Pharmacology, Emory University, Atlanta, Georgia 30322, and [4]Neuroscience Program, University of Science and Technology, Daejeon 305-701, Korea

In mammalian brain, neurons and astrocytes are reported to express various chloride and anion channels, but the evidence for functional expression of Ca^{2+}-activated anion channel (CAAC) and its molecular identity have been lacking. Here we report electrophysiological evidence for the CAAC expression and its molecular identity by mouse *Bestrophin 1* (*mBest1*) in astrocytes of the mouse brain. Using Ca^{2+} imaging and perforated-patch-clamp analysis, we demonstrate that astrocytes displayed an inward current at holding potential of −70 mV that was dependent on an increase in intracellular Ca^{2+} after $G_{\alpha q}$-coupled receptor activation. This current was mediated mostly by anions and was sensitive to well known anion channel blockers such as niflumic acid, 5-nitro-2(3-phenylpropylamino)-benzoic acid, and flufenamic acid. To find the molecular identity of the anion channel responsible for the CAAC current, we analyzed the expression of candidate genes and found that the mRNA for mouse *mBest1* is predominantly expressed in acutely dissociated or cultured astrocytes. Whole-cell patch-clamp analysis using HEK293T cells heterologously expressing full-length *mBest1* showed a Ca^{2+}-dependent current mediated by mBest1, with a complete impairment of the current by a putative pore mutation, W93C. Furthermore, mBest1-mediated CAAC from cultured astrocytes was significantly reduced by expression of *mBest1*-specific short hairpin RNA (shRNA), suggesting that the CAAC is mediated by a channel encoded by *mBest1*. Finally, hippocampal CA1 astrocytes in hippocampal slice also showed mBest1-mediated CAAC because it was inhibited by mBest1-specific shRNA. Collectively, these data provide molecular evidence that the mBest1 channel is responsible for CAAC function in astrocytes.

Introduction

In the brain, anions, including Cl^-, bicarbonate, and other organic anions, regulate various cellular events. A combination of transporters and ion channels are highly expressed in both neurons and glia to move these anions across membranes (Scott et al., 1995; Lambert and Oberwinkler, 2005; Kimelberg et al., 2006). Anion channels are classified as several families, including cystic fibrosis transport regulator, Ca^{2+}-activated anion channel (CAAC), volume-regulated anion channel (VRAC), and ClC channel, according to how they are activated (Kimelberg et al., 2006). The function of CAACs has been studied extensively because of their important role in excitable tissues, which require an increase in intracellular Ca^{2+} concentration ($[Ca^{2+}]_i$) for channel activity (Hartzell et al., 2005; Kunzelmann et al., 2007). CAAC is directly or indirectly activated by an increase in $[Ca^{2+}]_i$ and produces anion efflux or influx in mammalian cells and *Xenopus laevis* oocytes. This anion flux results in membrane depolarization or hyperpolarization, depending on the equilibrium potential for permeant anions (Hartzell et al., 2005). Whereas CAACs are previously known to be involved in the regulation of olfaction, taste, phototransduction, and excitability in the nervous system, the molecular identity and functional role of CAAC in the brain have not been well established.

At least seven different Cl^- or anion-mediated currents have been functionally characterized in astrocytes (Walz, 2002; Kimelberg et al., 2006), but direct evidence for the expression of Ca^{2+}-activated Cl^- current in astrocytes has been lacking. Astrocytes are actively involved in communication between neurons, and this role is mainly mediated by an increase in $[Ca^{2+}]_i$ secondary to activation of G-protein-coupled receptors (GPCRs) activated by neurotransmitter release from synaptic activity (Volterra and Meldolesi, 2005; Halassa et al., 2007). Thus, it is expected that astrocytic CAAC has an important role in astrocyte–neuron intercellular communication provided that the channel is functionally expressed in astrocytic membrane.

In this study, we investigated the functional expression of CAAC in astrocytes and identified a candidate gene encoding astrocytic CAAC current. Recently, *bestrophin-1* (*Best1*), which was initially cloned as the gene linked to the vitelliform macular dystrophy of Best, a juvenile form of macular degeneration, has

Received July 3, 2009; revised Sept. 7, 2009; accepted Sept. 9, 2009.

This work was supported by the Star Postdoctoral Fellowship (H.P), Ente Cassa di Risparmio Firenze (G.M.), Progetti de Rilevante Interesse Nazionale 2007 (G.M.), National Institutes of Health Grants NS39419 (S.F.T.) and NS43875 (C.J.L.), Korea Research Foundation Grant KRF-2005-070-C00096 (C.J.L.), and the Korea Institute of Science and Technology Core Competency Program (C.J.L.). We thank P. Lyuboslavsky and P. Le for their excellent technical assistance.

*H.P. and S.-J.O. contributed equally to this work.

Correspondence should be addressed to Dr. C. Justin Lee, Center for Neural Science, Convergence Technology Laboratory, Korea Institute of Science and Technology, 39-1 Hawolgok-Dong, Seongbuk-Gu, Seoul 136-791, Korea. E-mail: cjl@kist.re.kr.

DOI:10.1523/JNEUROSCI.3193-09.2009

 0270-6474/09/2913063-11$15.00/0

been suggested to encode a functional CAAC in non-neuronal tissue and peripheral neurons with an anion-selective pore and single-channel activity (Marmorstein et al., 2000; Sun et al., 2002; Eggermont, 2004; Qu et al., 2004; Chien et al., 2006; Pifferi et al., 2006; Kunzelmann et al., 2007; Hartzell et al., 2008). However, the expression profile and the function of bestrophin in the CNS have not been explored. To address this issue, we examined both the expression pattern of bestrophin family members and the possibility that these gene products might function as astrocytic CAAC. Our results demonstrate for the first time that astrocytes in both primary cell culture and *in situ* express functional CAAC encoded by *Best1*.

Materials and Methods

Cell culture, Ca^{2+} imaging, and electrophysiology. Cell cultures of human embryonic day HEK293T cells and mouse astrocytes were performed as described previously. For cultured astrocytes, mouse brain tissues containing cortex and hippocampus were isolated and dissociated mechanically. For Ca^{2+} imaging, cultured astrocytes were incubated with 5 μM fura-2 AM in 1 μM pluronic acid (Invitrogen) for 30 min at room temperature and subsequently transferred to a microscope stage for imaging using external solution (in mM: 150 NaCl, 10 HEPES, 3 KCl, 2 $CaCl_2$, 2 $MgCl_2$, and 5.5 glucose, pH 7.3). Intensity images of 510 nm wavelength were taken at 340 and 380 nm excitation wavelengths, and the two resulting images were taken for ratio calculations. Imaging Workbench software (INDEC BioSystems) was used for acquisition of intensity images and conversion to ratios. The extracellular recording solution for simultaneous Ca^{2+} imaging and perforated-patch-clamp recording contained the following (in mM): 150 NaCl, 10 HEPES, 3 KCl, 2 $CaCl_2$, 2 $MgCl_2$, and 5.5 glucose, pH 7.3. For perforated-patch-clamp recordings, the internal solution contained 25 μg/ml gramicidin D and the following (in mM): 75 Cs_2SO_4, 10 NaCl, 0.1 $CaCl_2$, and 10 HEPES, pH 7.1. Pipette resistances ranged from 5 to 8 MΩ. It took 20–30 min to achieve acceptable perforation, with final series resistances ranging from 15 to 40 MΩ. In whole-cell patch clamp, patch pipettes that have 3–6 MΩ of resistance are filled with the standard intracellular solution (see below). Current–voltage curves were established by applying 100-, 200-, or 1000-ms-duration voltage ramps from −100 to +100 mV. Data were acquired by an Axopatch 200A amplifier controlled by Clampex 9.2 via Digidata 1322A data acquisition system (Molecular Devices). Experiments were conducted at room temperature (20–24°C). The pipette solution for whole-cell patch clamp in astrocytes contained the following (in mM): 135 CsCl, 5 $MgCl_2$, 5 EGTA, 10 HEPES, and 10 glucose, pH 7.3, adjusted with CsOH. To activate CAAC or mouse Best1 (mBest1) directly, we applied high Ca^{2+}-containing intracellular patch pipette solution to cultured astrocytes or mBest1-expressing HEK293T cells, which contained the following (in mM): 146 CsCl, 5 (Ca^{2+})–EGTA–*N*-methyl-D-glucamine (NMDG), 2 $MgCl_2$, 8 HEPES, and 10 sucrose, pH 7.3, adjusted with NMDG. For control experiments, we used Ca^{2+}-free intracellular solution composed of the following (in mM): 146 CsCl, 5 EGTA–NMDG, 2 $MgCl_2$, 8 HEPES, and 10 sucrose, pH 7.3, adjusted with NMDG. The concentration of free $[Ca^{2+}]_i$ in the solution was determined as described. The extracellular solution contained the following (in mM): 150 NaCl, 10 HEPES, 3 KCl, 2 $CaCl_2$, 2 $MgCl_2$, and 5.5 glucose, pH 7.3 with NaOH (~320 mOsm). In some experiments, the bath and pipette solutions for mBest1-expressing HEK293T cells to activate Cl^- current were prepared as described previously (O'Driscoll et al., 2009). The extracellular solution contained the following (in mM): 126 NaCl, 10 HEPES, 20 glucose, 1.8 $CaCl_2$, 1.2 $MgCl_2$, and 10 tetraethylammonium (TEA)-Cl, pH was set to 7.35, adjusted with NaOH. The pipette solution was composed of the following (in mM): 20 TEA-Cl, 106 CsCl, 8.7 $CaCl_2$, 5 HEPES, 10 BAPTA, 3 MgATP, 0.2 GTP-Li, and 0.5 $MgCl_2$, pH 7.2 adjusted with CsOH. Relative permeability of the channels was determined by measuring the shift in E_{rev} after changing the bath solution from one containing 161 mM Cl^- to another with 150 mM *X* and 11 mM Cl^-, where *X* is the substituted anion. We used an agar bridge to prevent any nonspecific holding potential shift caused by a replacement of Cl^- with different anions. The permeability ratio, P_X/P_{Cl^-}, was estimated using the modified Goldman–Hodgkin–Katz equation as reported previously (Qu et al., 2004):

$$P_X/P_{Cl^-} = [Cl^-]_i/\{[X]_o \exp(\Delta E_{rev}F/RT)\} - [Cl^-]_o/[X]_o.$$

In slice patch experiments, transverse brain slices (300–400 μm) containing hippocampus (from at least three 6- to 8-week-old B6 mice) were prepared as described previously (Lee et al., 2007). Sulforhodamine-101 (SR-101) (1 μM; Sigma) dye was loaded into acute brain slice as described previously (Kafitz et al., 2008). Prepared slices were left to recover for at least 1 h before recording in oxygenated (95% O_2 and 5% CO_2) artificial CSF (ACSF) (in mM: 130 NaCl, 24 $NaHCO_3$, 3.5 KCl, 1.25 NaH_2PO_4, 1 $CaCl_2$, 3 $MgCl_2$, and 10 glucose, pH 7.4). Because SR-101-loaded cells from hippocampal CA1 stratum radiatum region showed typical properties of astrocytes, such as passive current response and absence of depolarization-evoked action potential responding to voltage step command (from −100 to +100 mV) (see Fig. 7*B*), we used this dye for identifying hippocampal astrocytes. The standard ACSF recording solution was composed of the following (in mM): 130 NaCl, 24 $NaHCO_3$, 3.5 KCl, 1.25 NaH_2PO_4, 1.5 $CaCl_2$, 1.5 $MgCl_2$, and 10 glucose, pH 7.4 (saturated with 95% O_2 and 5% CO_2). For hypertonic ACSF, sucrose was added to increase the osmolarity of standard recording ACSF up to ~15% (Takano et al., 2005). Pipette solution contained the following (in mM): 60 KCl, 73 K-gluconate, 1 $MgSO_4$, and 10 HEPES, pH 7.3 adjusted with KOH. For Cs-containing pipette solution, an equimolar concentration of potassium was replaced with cesium (CsCl and Cs-gluconate). Experiments with a holding current more than −100 pA were rejected.

Reverse transcription-PCR and single-cell PCR. Total RNA was prepared from whole brain of adult mice (C57BL/6, 3–4 weeks old) or cultured astrocyte from postnatal day 0–3 mice using Trizol reagent (Invitrogen). cDNA was synthesized using Super Script III reverse transcriptase (Invitrogen). The reverse transcription (RT)-PCR primers used to check expression of mBest1, mBest2, and mBest3 from brain or cultured astrocyte cDNA were as followings: mBest1 forward, 5′-AGGACGATGATGATTTTGAG-3′ and mBest1 reverse, 5′-CTTTCTGGTTTTTCTGGTTG-3′; mBest2 forward, 5′-TCGTCTACACCCAGGTAGTC-3′ and mBest2 reverse, 5′-GAAAGTTGGTCTCAAAGTCG-3′; mBest3 forward, 5′-AAAGGCTACGTAGGACATGA-3′ and mBest3 reverse, 5′-GAAAGGACGGTATGCAGTAG-3′. To test the presence of other CAAC candidates in mouse brain or astrocyte, the following primer sets were used: mouse Cl^- channel-calcium activated 1 (mCLCA1), mCLCA2, mCLCA4 forward, 5′-TTCAAGATCCAAAAGGAAAA-3′ and mCLCA1, mCLCA2, mCLCA4 reverse, 5′-GCTCAGTCTGGTTTTGTTTC-3′; mCLCA5 forward, 5′-TAAGATTCCAGGGACAGCTA-3′ and mCLCA5 reverse, 5′-AAAGGAGGAAAAATACCTGG-3′; mouse *Drosophila* tweety homolog 1 (mTtyh1) forward, 5′-AGACACCTATGTGCTGAACC-3′ and mTtyh1 reverse, 5′-AGAAAAGAGCATCAGGAACA-3′; mTtyh2 forward, 5′-CCAGCTTCTGCTAAACAACT-3′ and mTtyh2 reverse, 5′-AATCTCTGTCCCTGTTGATG-3′; mTtyh3 forward, 5′-CAGTACTGAGTGGGGACATT-3′ and mTtyh3 reverse, 5′-CTGTGACAAAGGAGAAGAGG-3′. To perform single-cell RT-PCR, a single astrocyte and neuron was acutely and mechanically dissociated from cortex of adult mouse brain. The cDNA of single, dissociated cells was amplified using Sensiscript RT kit (Qiagen). Neuron-specific enolase (NSE) (300 bp) and glial fibrillary acidic protein (GFAP) (360 bp) were used to identify the harvested cell type. PCR amplification was performed using the following primers: mBest1 forward outer primer, 5′-AGGACGATGATGATTTTGAG; mBest1 forward inner primer, 5′-ACCTTCAACATCAGCCTAAA-3′; mBest1 reverse common primer, 5′- CTTTCTGGTTTTTCTGGTTG-3′; NSE forward common primer, 5′- GCTGCCTCTGAGTTTTACCG-3′; NSE reverse outer primer, 5′- GAAGGGGATCACAGCACACT-3′; NSE reverse inner primer, 5′-CTGATTG ACCTTGAGCAGCA-3′; GFAP forward outer primer, 5′-GAGGCAGAAGCTCCAAGATG-3′; GFAP forward inner primer, 5′-AGAACAACCTGGCTGCGTAT-3′; GFAP reverse common primer, 5′-CGGCGATAGTCGTTAGCTTC-3′. The first PCR amplification was performed as described below. Samples were heated to 94°C for 5 min. Each cycle consisted of denaturation at 94°C for 30 s, annealing at 50°C for 30 s, and elongation at 72°C for 30 s. Forty-two cycles were performed with a programmable thermocycler (Eppendorf). The second PCR condi-

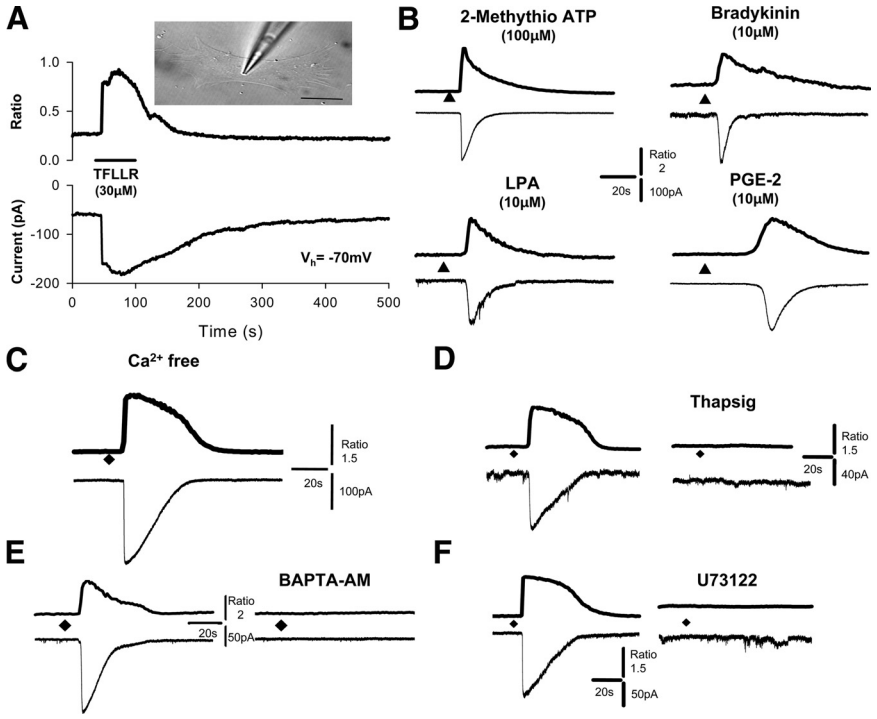

Figure 1. Ca^{2+}-dependent current in cultured astrocyte. ***A***, Inset, A representative image of a gramicidin-D perforated-patch-clamp recording from fura-2 AM-loaded cultured astrocyte. Scale bar, 20 μm. Representative simultaneous recordings are shown for 30 μM TFLLR-induced changes in intracellular Ca^{2+} transients (top trace) and an inward current in cultured fura-2 AM-loaded astrocytes (bottom trace; holding potential V_h of −70 mV). ***B***, Multiple astrocytic GPCR agonists induced Ca^{2+}-activated inward currents. Simultaneous monitoring of the intracellular Ca^{2+} concentration (top trace) and whole-cell current (bottom trace) using perforated-patch recordings in response to 2-methylthio-ATP (100 μM; $n = 9$), bradykinin (10 μM; $n = 8$), LPA (10 μM; $n = 2$), and PGE2 (10 μM; $n = 2$). ***C–F***, Astrocytic Ca^{2+}-activated inward currents are dependent on internal Ca^{2+} increase. TFLLR-induced Ca^{2+} and current responses under perforated-patch-clamp mode were intact in Ca^{2+}-free extracellular bath ($n = 5$; ***C***). TFLLR-induced Ca^{2+} and current responses were inhibited by preincubation with 100 nM thapsigargin for 5 min ($n = 5$; ***D***), 50 μM BAPTA-AM for 30 min ($n = 5$; ***E***), or 2 μM U73122 for 10 min ($n = 5$; ***F***). TFLLR was applied at time denoted by ▲, ◆; application duration was 10 s.

tion consisted of denaturation at 94°C for 30 s, annealing at 55°C for 30 s, elongation at 72°C for 30 s for 42 cycles, and subsequent cooling to 4°C until analysis.

Cloning of mBest1, mutagenesis, and expression. For the cloning of full-length *mBest1* cDNA, total RNA was purified from cultured astrocytes or testis from adult male mice (C57BL/6), and cDNA was synthesized. Using 21 base primer pair spanning the open reading frame based on National Center for Biotechnology Information database cDNA (GenBank accession number NM_011913.2), PCR was performed to acquire the full-length open reading frame of *mBest1*. Resulting PCR products were cloned into a pGEM-T easy vector (Promega) and sequenced to be verified. To express *mBest1* in mammalian cells, *mBest1* full-length fragment from pGEM-T easy plasmid (6.65 kb) was subcloned into pIRES2–DsRed (Invitrogen) by using XbaI and XmaI sites. The pIRES2–mBest1–DsRed plasmid was transfected into HEK293T cells using Effectene transfection reagent (Qiagen). Approximately 12 h after transfection, cells were replated onto glass coverslips for electrophysiological recording. Transfected cells were used for patch-clamp experiments within 12 h. *mBest1* pore mutant (mBest1–W93C) and short hairpin RNA (shRNA)-insensitive mutant constructs (*mBest1* shRNA-insensitive mutant) were generated by using PCR-based site-directed mutagenesis kit (Stratagene). PCR primers for mutagenesis of mBest1–W93C included the following: mBest1 g279c sense, 5′-GGTGAGCCGCTGCTGGAGCCAGTAC-3′; mBest1 g279c antisense, 5′-GTACTGGCTCCAGCAGCGGCTCACC-3′. PCR primers for mutagenesis of *mBest1* shRNA-insensitive mutant constructs were as follows: c567t_c570t_t571c_a576c sense, 5′-GTGCCCTGGGTGTGGTTTGCTAATCTGTCCATGAAGGCCTATCTTGGAGG-3′; c567t_c570t_t571c_a576c antisense, 5′-CCTCCAAGATAGGCCTTCATGGACAGATTAGCAAACCACACCCAGGGCAC-3′.

mBest1 shRNA and lentivirus production. The *mBest1* nucleotides from 774 to 793 (5′-tttgccaacttgtcaatgaa-3′) was selected for target region of *mBest1* shRNA. For lentivirus-based shRNA expression, *mBest1* shRNA was synthesized as follows: 5′- tttgccaacttgtcaatgaattcaagagatcattgacaagttggcaatttttc-3′ and 5′-tcgagaaaaaatcgcatagcgtatgccgtttctcttgaaaacggcatacgctatgcgaa-3′. The annealed double-stranded oligo was inserted into HpaI–XhoI restriction enzyme sites of pSicoR lentiviral vector (Addgene, Ventura et al., 2004) and verified by sequencing. Scrambled shRNA-containing pSicoR construct was used as control. shRNA-containing pSicoR was electroporated into cultured astrocytes (MicroPorator; Digital Bio). For shRNA expression into hippocampal region, lentivirus (produced by Macrogen) was delivered into the hippocampal CA1 region by the stereotaxic surgery method (Cetin et al., 2006).

In situ *hybridization.* To make specific riboprobes for mRNA of *mBest1*, we cloned partial cDNA fragments of *mBest1*. Primers were as follows: forward, 5′- ACCTTCAACATCAGCCTAAA-3; reverse, 5′-CTTTCTGGTTTTTCTGGTTG-3′. The plasmid was linearized and used for *in vitro* transcription (Roche Diagnostics) to label RNA probes with digoxigenin–UTP. *In situ* hybridization was performed as described previously with some modifications (Hougaard et al., 1997; Kadkol et al., 1999). Frozen brains of adult mice were sectioned at 20 μm thickness on a cryostat. The sections were then fixed in 4% paraformaldehyde, washed with PBS, and acetylated for 10 min. The sections were incubated with the hybridization buffer (50% formamide, 4× SSC, 0.1% 3-[(3-cholamidopropyl)dimethylammonio]-1-propanesulfonate, 5 mM EDTA, 0.1% Tween 20, 1.25× Denhardt's solution, 125 μg/ml yeast tRNA, and 50 μg/ml heparin) and digoxigenin-labeled probes (200 ng) for 18 h at 60°C. Nonspecific hybridization was removed by washing in 2× SSC for 10 min and in 0.1× SSC at 50°C for 15 min. For immunological detection of digoxigenin-labeled hybrids, the sections were incubated with anti-digoxigenin antibody conjugated with alkaline phosphatase (Roche Diagnostics) for 1 h, and the color reaction was performed with 4-nitroblue tetrazolium chloride/bromo-4-chloro-3-indolyl phosphate (Sigma). Sections were dehydrated and mounted with Vectamount (Vector Laboratories).

Immunohistochemistry. Rabbit polyclonal mBest1 IgG was produced using antigen described previously (Barro Soria et al., 2006) (Ab Frontier). B6 adult mice were deeply anesthetized by 2% avertin and perfused with room temperature 0.1 M PBS, followed by ice-cold 4% paraformaldehyde. Brains were postfixed in 4% paraformaldehyde at 4°C for 24 h and 30% sucrose 4°C for 48 h. Brains were then cut in coronal sections of 30 μm on a cryosection. Sections were blocked in 0.1 M PBS containing 0.3% Triton X-100 (Sigma) and 2% serum from species of the secondary antibody for 1 h. Primary antibody was then applied at appropriate dilution [mBest1 IgG at 1:200, GFAP at 1:200 (Millipore Bioscience Research Reagents), neuronal-specific nuclear protein (NeuN) at 1:200 (Millipore Bioscience Research Reagents)] and incubated overnight at 4°C. After overnight incubation, the sections were washed three times in PBS and then incubated in secondary antibody [Alexa 488 goat anti-rabbit IgG at 1:400 (Invitrogen), tetramethylrhodamine isothiocyanate-conjugated goat anti-chicken IgG at 1:100 (The Jackson Laboratory), and Alexa 555 goat anti-mouse IgG (Invitrogen) for 2 h]. After three rinses in PBS, the sections were mounted on slide glass. Images were acquired on an Olympus Fluoview FV1000 confocal microscope and analyzed using NIH Image J software.

Results

Astrocytes express Ca^{2+}-activated current

Previous studies have provided ample experimental evidence for functional expression of anion channels in astrocytes (Walz, 2002), but there is only a limited number of reports describing functional expression or properties of CAAC in astrocytes of the CNS (Crépel et al., 1998; Walz, 2002; Parkerson and Sontheimer, 2004; Takano et al., 2005; Abdullaev et al., 2006; Ramos-Mandujano et al., 2007). Therefore, we examined whether astrocytes express functional CAAC. We simultaneously recorded whole-cell currents and intracellular Ca^{2+} responses in cultured astrocytes from mouse brain under the gramicidin-D perforated-patch configuration (Fig. 1*A*), which allowed us to minimize dialysis of intracellular anions (Kyrozis and Reichling, 1995). An astrocyte that was well isolated from other cells in culture was selected for recording to avoid gap-junction coupling that might compromise our ability to control the voltage. Because astrocytic G-protein (G_q or $G_{12/13}$)-coupled receptors, such as protease activated receptor-1 (PAR-1), are known to induce a transient increase in the $[Ca^{2+}]_i$ (Porter and McCarthy, 1997; Lee et al., 2007), we applied the PAR-1-selective peptide agonist TFLLR (TFLLR-NH_2) (Lee et al., 2007) to test whether a PAR1-stimulated increase in $[Ca^{2+}]_i$ in astrocyte caused any changes in membrane conductance. During application of 30 μM TFLLR (threefold EC_{50}), we observed a large inward current that closely followed the time course of the Ca^{2+} response (154 ± 16 pA, mean ± SEM; $n = 26$) (Fig. 1*A*). This result raised the possibility of functional expression of CAAC in astrocytes. When other types of G_q-protein-coupled receptors, such as P2Y receptor, bradykinin receptor, lysophosphatidic acid (LPA) receptor, and prostaglandin E2 (PGE2) receptor, were activated by corresponding selective agonists, similar concomitant increase of $[Ca^{2+}]_i$ and inward current were observed (Fig. 1*B*), indicating that this current induction is a general mechanism shared by a host of astrocytic G_q-protein-coupled receptors.

CAAC is known to be activated by submicromolar physiological range of cytosolic Ca^{2+} and shows anion selectivity and outwardly rectifying current, which are blocked by anion channel blockers (Eggermont, 2004). To test whether the inward current we detected in astrocytes is mediated by CAAC, we first examined the Ca^{2+} dependency of TFLLR-induced current. TFLLR-induced inward current was intact in Ca^{2+}-free bath (Fig. 1*C*) but was eliminated by BAPTA-AM treatment (Fig. 1*E*). Impairment of the Ca^{2+} release from internal stores by previous application of either thapsigargin (Fig. 1*D*) or phospholipase C inhibitor, U73122 (1-[6((17β)-3-methoxyestra-1,3,5(10)-trien-17-yl)amino)hexyl]-1*H*-pyrrole-2,5-dione) (Fig. 1*F*), also impaired both the TFLLR-induced $[Ca^{2+}]_i$ increase and the inward current, indicating a dependency to Ca^{2+} release from intracellular stores.

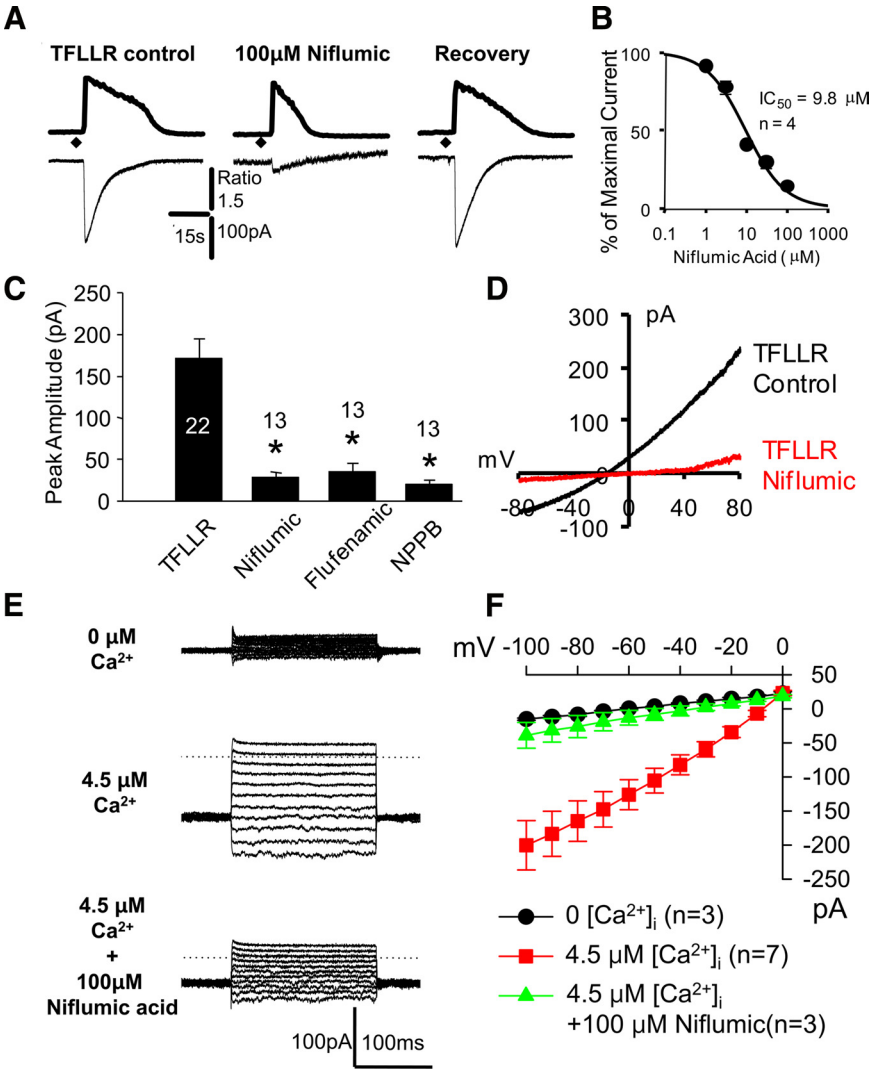

Figure 2. Astrocytic Ca^{2+}-dependent current is sensitive to anion channel blocker. ***A***, Representative TFLLR-induced inward current responses recording perforated-patch-clamp mode were measured in the absence or presence of 100 μM niflumic acid in the same cell ($n = 5$). TFLLR was applied at time denoted by ◆; application duration was 10 s. ***B***, The concentration–response relationship for niflumic acid block of Ca^{2+}-activated current is shown. ***C***, The anion channel blockers 100 μM niflumic acid, 100 μM flufenamic acid, and 100 μM NPPB all inhibit TFLLR-induced current. Each bar represents the mean ± SEM; one-way ANOVA with Tukey's *post hoc* test; *$p < 0.05$ versus TFLLR-treated group. ***D***, The *I–V* curve was generated by subtracting the response to 1 s voltage ramp traces before and during TFLLR-induced current responses. *I–V* curve during 100 μM niflumic acid treatment shows voltage-independent block of the current by niflumic acid. ***E***, Representative current recording traces show direct activation of an inward current that is sensitive to niflumic acid from a single astrocyte that was placed under whole-cell patch voltage clamp with an internal solution initially containing 0 μM and subsequently 4.5 μM Ca^{2+}. This Ca^{2+}-induced current was inhibited by treatment of niflumic acid in the same cell. ***F***, Summary of the *I–V* relationship established in the presence of 0 μM Ca^{2+}, 4.5 μM Ca^{2+}, and 4.5 μM Ca^{2+} with 100 μM niflumic acid present in the extracellular solution.

Astrocytic Ca^{2+}-activated current is dependent on anion channel activation

We next tested whether this inward current is mediated by an anion channel. Perforated-patch-clamp measurement showed that $[Ca^{2+}]_i$-activated inward current was blocked by treatment of a series of anion channel blockers, including 100 μM niflumic acid, 100 μM flufenamic acid, and 100 μM 5-nitro-2(3-

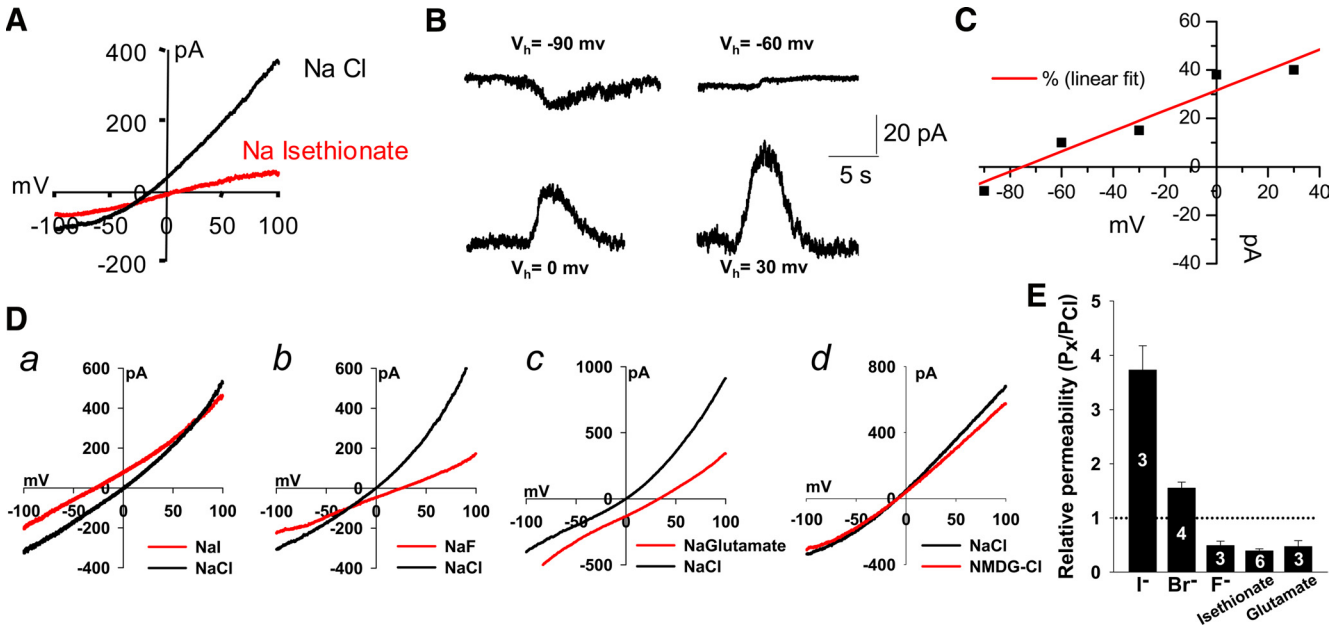

Figure 3. Anion permeability of TFLLR-induced inward current. ***A***, The *I–V* curves for TFLLR-induced current responses were recorded under perforated-patch-clamp mode, with the chloride ion (150 mM NaCl) in external bath exchanged with isethionate (150 mM Na-isethionate) in the same cell. ***B***, TFLLR-induced current responses under whole-cell patch configuration with a Cs-gluconate (7 mM Cl^-) containing internal solution are shown at various holding potentials (V_h of −90 to +40 mV). ***C***, The *I–V* relationship of the current responses shown in ***B***. The predicted reversal potential from linear regression was −71 ± 1.5 mV ($n = 4$), which agreed well with the calculated reversal potential of −75 mV. ***D***, Representative *I–V* curves for TFLLR-induced current responses recorded under whole-cell patch-clamp configuration using 4.5 μM Ca^{2+} containing CsCl (150 mM) are shown for solutions in which chloride ion (150 mM NaCl) in the external was exchanged bath with I^- (***a***), Br^- (***b***), and F^- (***c***). To test the permeability of Na^+, the *I–V* curves for TFLLR-induced current responses were recorded under perforated-patch-clamp mode, and Na^+ (150 mM NaCl) was exchanged with $NMDG^+$ (***d***). *I–V* curves from ion-substituted group are shown as red curves. ***E***, Relative permeability ratios (P_X/P_{Cl}) of TFLLR-induced currents are summarized. P_X/P_{Cl} was calculated from the Goldman–Hodgkin–Katz equation (see Materials and Methods). Relative permeability of large anions such as isethionate and glutamate were also included. Numbers of determinations are indicated on the bar graph.

phenylpropylamino)-benzoic acid (NPPB) (Qu and Hartzell, 2001; Hartzell et al., 2005) (Fig. 2*A*,*C*). Niflumic acid-mediated block of the TFLLR-induced current was voltage independent (Fig. 2*D*), with an IC_{50} of 9.8 μM (Fig. 2*B*), virtually identical to that reported for CAACs expressed in *Xenopus laevis* oocytes (IC_{50} of 10.1 μM) (Qu and Hartzell, 2001). In addition, we were able to directly induce an increase in conductance in astrocytes by a membrane rupture for whole-cell mode with internal solutions containing high free $[Ca^{2+}]_i$ (~4.5 μM) (Qu et al., 2004). The current induced by this manipulation displayed a nondesensitizing time course and was readily blocked by treatment of 100 μM niflumic acid (Fig. 2*E*,*F*) and 100 μM NPPB ($n = 3$) (data not shown). On the contrary, carbenoxolone (100 μM; $n = 3$) or chlorotoxin (1 μM; $n = 2$) treatment of astrocytes did not block this current, suggesting that gap-junction hemichannels or chlorotoxin-sensitive chloride channels are not involved in this Ca^{2+}-activated current (data not shown) (Dalton et al., 2003; Ye et al., 2003). These results demonstrated that astrocytes display Ca^{2+}-activated current that is readily blocked by anion channel blockers.

Anion selectivity of astrocytic CAAC

We subsequently tested whether the astrocytic Ca^{2+}-activated inward current recorded under gramicidin-D perforated-patch configuration was carried by anions. We determined the current–voltage (*I–V*) relationship with a voltage ramp protocol for the TFLLR-induced current in astrocytes in the presence of extracellular Cl^- or with extracellular Cl^- replaced by the larger and presumably less permeable isethionate (Fig. 3*A*). The reversal potential in perforated-patch recordings was significantly shifted to the right, from −13.2 ± 1.9 to + 5.4 ± 1.5 mV ($n = 8$ and 5, respectively; $p < 0.05$, unpaired *t* test), suggesting that this current was carried by anions. In a separate experiment, the reversal potential of the TFLLR-induced current under whole-cell configuration with the intracellular solution containing 7 mM Cl^- was −71 ± 1.5 mV ($n = 4$) (Fig. 3*B*,*C*), which agreed well with the calculated reversal of −75 mV, according to the Nernst equation.

To determine the relative permeability to different anions, a series of ion substitution experiments was performed under whole-cell patch-clamp mode with internal solution containing a high concentration of Ca^{2+}. The Cl^- of external bath solution was substituted with I^-, Br^-, or F^-, and the *I–V* relationship of astrocytic CAAC was determined. We found that astrocytic CAAC showed outwardly rectifying *I–V* relationship and displayed the relative permeability order of $I^- > Br^- > Cl^- > F^-$ (Fig. 3*D*,*E*), which was identical to the previously known properties of other CAACs reported in *Xenopus laevis* oocytes and mammalian cells (Cliff and Frizzell, 1990; Clapp et al., 1996; Kuruma and Hartzell, 1999). The astrocytic CAAC also showed a significant permeability to large anions such as glutamate and isethionate (Fig. 3*Dc*,*E*), as previously reported for aspartate in *Xenopus laevis* oocytes (Qu et al., 2003). However, ion substitution of Na^+ ion by an exchange of NaCl with NMDG-Cl did not change the reversal potential ($n = 5$; $p = 0.66$, unpaired *t* test), indicating that Na^+ ion is the minimal charge carrier of CAAC current in astrocyte. Together, these results are consistent with the idea that astrocytes express functional CAACs, which can be activated by an increase in cytosolic Ca^{2+} from internal Ca^{2+} store during GPCR activation.

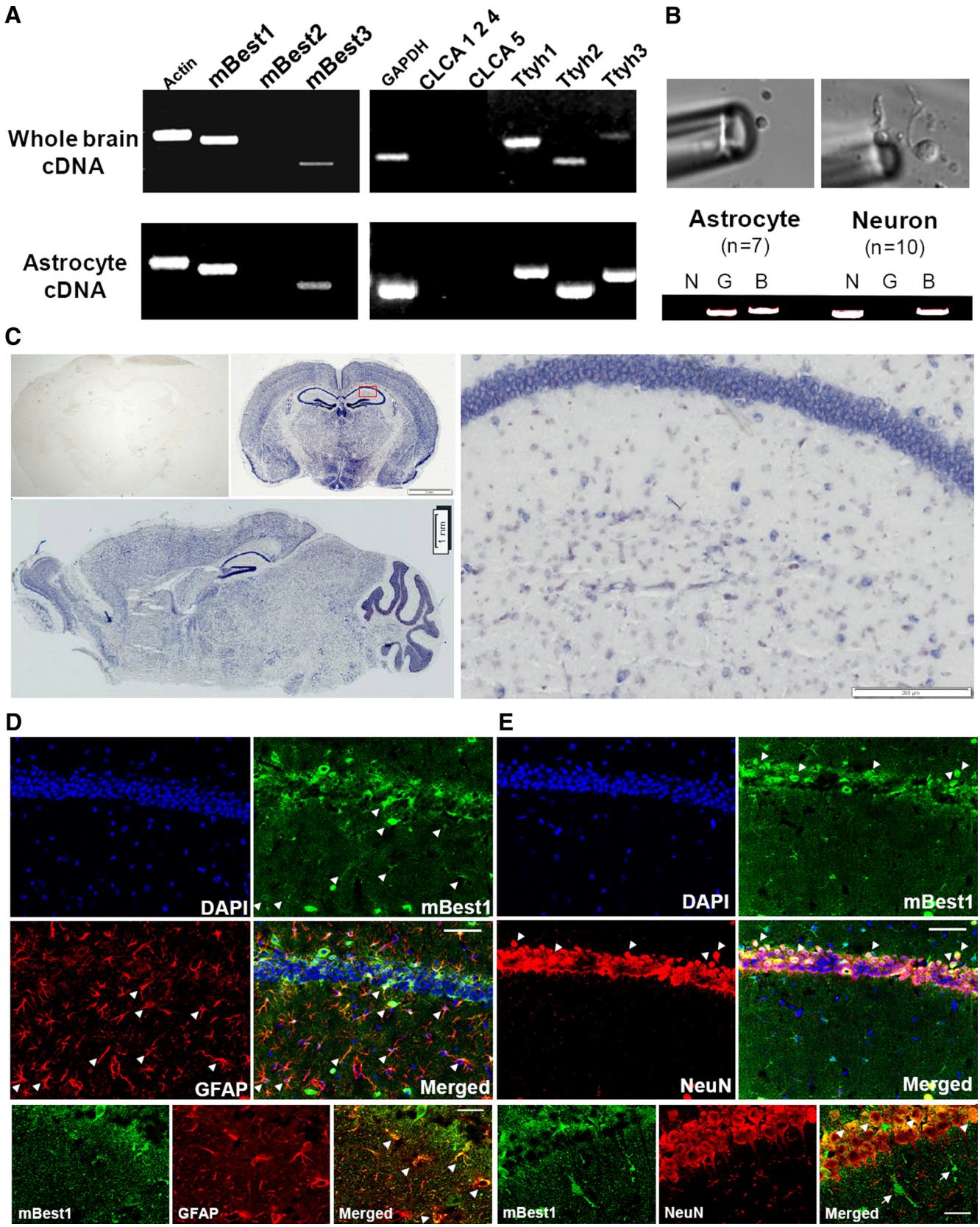

Figure 4. Brain expression of bestrophin genes. ***A***, RT-PCR analysis of the expression of CAAC candidate genes. The expression profiles of CAAC candidate genes such as *CLCA* (*CLCA1*, *CLCA2*, *CLCA4*, and *CLCA5*), mouse *tweety* family genes (*Ttyh1*, *Ttyh2*, and *Ttyh3*), and mouse *bestrophin* genes (*mBest1*, *mBest2*, and *mBest3*) were examined using cDNAs from whole mouse brain (Whole brain cDNA) or cultured astrocytes (Astrocyte cDNA). β-Actin (Actin) and glyceraldehyde 3-phosphate dehydrogenase (GAPDH) was used as a control. PCR products of each gene were from the same number of PCR cycles. ***B***, Representative single-cell RT-PCR analysis. Mouse brain cortex was dissociated, and isolated single-cell PCR was used to amplify the target cDNAs. Primer sets were used for detecting *NSE* (N), *GFAP* (G), and *mBest1* (B) to confirm cell phenotype. ***C***, *In situ* hybridization analysis for detecting endogenous *mBest1* transcript in whole-brain region. *In situ* hybridization results from coronal (top middle) and sagittal section (bottom left) using antisense probe for *mBest1* mRNA. A higher-magnification view of boxed area (red box) in stratum radiatum in (*Figure legend continues.*)

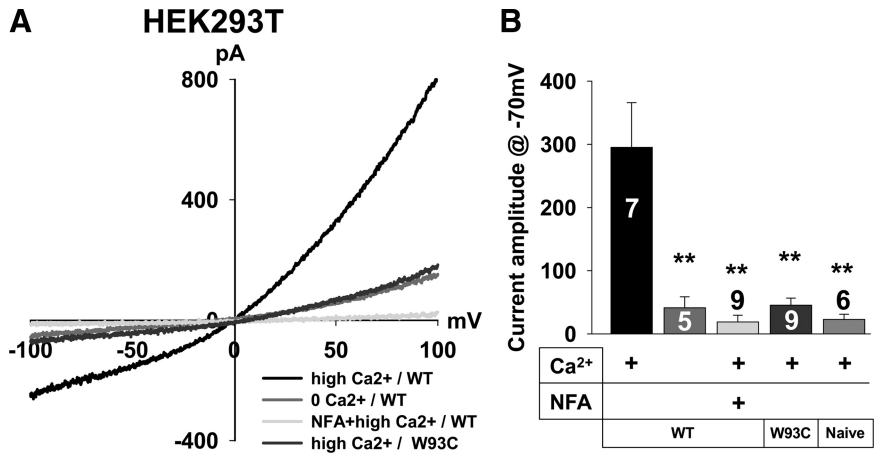

Figure 5. mBest1 forms a bona fide CAAC. ***A***, Representative *I–V* responses of HEK293T cells expressing wild-type (WT) mBest1 (mBest1) or mBest1–W93C mutant under whole-cell patch-clamp configuration using 4.5 μM Ca^{2+}-containing or 0 Ca^{2+}-containing patch pipette solution. ***B***, Bar graph showing summary of current amplitudes recorded at a holding potential of −70 mV (mean ± SEM). The anion channel blocker niflumic acid (NFA; 100 μM) was preincubated with cells for 10 min. Vector-expressing HEK293T cells (Naive) were tested for measuring Ca^{2+}-induced current response as a control. Numbers of determinations are indicated on the bar graph. $^{**}p < 0.01$ versus mBest1-expressing cells with 4.5 μM Ca^{2+} pipette solution, one-way ANOVA with Dunnett's multiple comparison test.

Identification of the gene responsible for CAAC in mouse astrocyte

Molecular identification of anion channels has been hampered by the lack of specific blockers. CAAC is the one of very few channels for which a cDNA has not yet been unequivocally identified (d'Anglemont de Tassigny et al., 2003; Eggermont, 2004). To identify the genes encoding CAAC channels in astrocytes, we performed RT-PCR with primer sets for various CAAC candidate genes, such as *CLCA*, *Ttyh*, and *Best* family genes (Eggermont, 2004; Suzuki and Mizuno, 2004). Our RT-PCR analysis demonstrated that *mBest1*, *mBest3*, and *mTtyh1–mTtyh3* were significantly expressed, whereas those for CLCA were absent in the brain and cultured astrocytes (Fig. 4*A*). Despite the significant expression in astrocytes, mouse *Ttyh* family genes were not considered as the astrocytic CAAC candidate attributable to the non-overlapping properties such as insensitivity to niflumic acid and the lack of outward rectified current–voltage relationship (Suzuki and Mizuno, 2004). Although the expression levels of *mBest1* and *mBest3* in cultured astrocytes were slightly lower than other tissues such as testis and heart (supplemental Fig. 1, available at www.jneurosci.org as supplemental material) (Marmorstein et al., 2000; Pifferi et al., 2006), it was evident that *mBest1* was significantly expressed with higher levels than *mBest3* in astrocytes (Fig. 4*A*) (supplemental Fig. 1, available at www.jneurosci.org as supplemental material). Therefore, *mBest1* appeared to be an appropriate candidate gene for astrocytic CAAC.

We next analyzed the expression pattern of *mBest1* within the brain by cell type and by brain region. By performing single-cell RT-PCR using a *mBest1*-specific primer set and cDNA of individual acutely dissociated astrocytes or neurons from adult mouse cortex, we identified the expression of *mBest1* in both *GFAP*- and *NSE*-expressing cell types (Fig. 4*B*), indicating that *mBest1* is expressed in both astrocytes and neurons. *In situ* hybridization analysis also showed a widely distributed expression pattern of *mBest1* mRNA with higher level in olfactory bulb, hippocampus, and cerebellum and significant expression in both neuron and astrocyte-like cells (Fig. 4*C*). To confirm the expression of mBest1 protein in mouse hippocampus, immunohistochemical analysis using *mBest1*-specific antibody (Barro Soria et al., 2006) was performed. Consistent with single-cell RT-PCR and *in situ* hybridization analysis, mBest1 protein showed significant expression in both NeuN- and GFAP-positive cells (Fig. 4*D*,*E*). Together, these results demonstrate for the first time the astrocytic and neuronal expression of *mBest1* in the brain.

Heterologously expressed mBest1 displays CAAC function

Recently, it has been reported that heterologously expressed *mBest1* displays CAAC current by whole-cell patch-clamp recordings using submicromolar Ca^{2+} containing patch pipette internal solution. Consistent with this report, we observed that heterologously expressed *mBest1* in HEK293T cells displayed Ca^{2+}-induced outwardly rectifying current, which was mostly inhibited by pretreatment with niflumic acid or by using a pipette internal solution lacking Ca^{2+} (Fig. 5*A*,*B*) (current amplitude at V_h of −70 mV; mBest1 expression with high Ca^{2+}, 295 ± 71 pA, $n = 7$; mBest1 expression without Ca^{2+}, 41 ± 17 pA, $n = 5$; niflumic acid pretreated mBest1 with high Ca^{2+}, 19 ± 11 pA, $n = 9$; $^{**}p < 0.01$ vs mBest1 expression with high Ca^{2+} group; one-way ANOVA with Dunnett's multiple comparison test). To verify whether mBest1 forms an ion channel, we constructed an anion-selective pore mutant of mBest1 by mutating tryptophan-93 to cysteine (W93C), which has been suggested to reside within the anion-selective pore region in *mBest2* channel. Because this presumed pore-forming residue is conserved between *mBest1* and *mBest2* (Qu and Hartzell, 2004; Qu et al., 2006b), we hypothesized that W93C mutation of *mBest1* should impair the CAAC current when heterologously expressed in HEK293T cells. As expected, we found that *mBest1–W93C* expressing HEK293T cells did not show any significant CAAC current using a high Ca^{2+}-containing pipette internal solution (Fig. 5*A*,*B*) (current amplitude at V_h of −70 mV; *mBest1–W93C* expression with high Ca^{2+}, 45 ± 11 pA, $n = 9$; $^{**}p < 0.01$ vs *mBest1* expression with high Ca^{2+} group; one-way ANOVA with Dunnett's multiple comparison test). These data suggest that heterologously expressed *mBest1* encodes a Ca^{2+}-activated anion channel with a pore similar to *mBest2*.

mBest1 expression in cultured astrocytes is responsible for CAAC current

To determine the molecular identity of astrocytic CAAC as *mBest1*, we designed an *mBest1*-specific shRNA (*mBest1*–shRNA) to selectively knockdown the expression of *mBest1* transcript. Our semi-quantitative RT-PCR analysis showed that the expression of *mBest1*-shRNA resulted in effective and selective knockdown of endogenous *mBest1* mRNA in cultured astrocytes (Fig. 6*A*), suggesting that *mBest1*–shRNA could effectively knockdown

←

(*Figure legend continued.*) CA1 region of coronal section (right). *In situ* hybridization result using sense probe for *mBest1* in coronal section (top left) was shown as a negative control. ***D***, ***E***, Immunohistochemical analysis of mBest1 expression in GFAP-positive (***D***) or NeuN-positive (***E***) cells in hippocampal CA1 region. Arrowheads indicate the colocalization of GFAP (***D***) or NeuN (***E***) with mBest1. Scale bar, 50 μm. Bottom panels show higher magnification of top panels. Scale bar, 10 μm. DAPI, 4′,6′-Diamidino-2-phenylindole.

the expression of CAAC current. We subsequently recorded astrocytic CAAC current in scrambled shRNA- or *mBest1*–shRNA-expressing cultured astrocytes using perforated-patch-clamp mode to test whether *mBest1* encodes astrocytic CAAC current. We found that CAAC current in cultured astrocyte was significantly suppressed by *mBest1*–shRNA expression (Fig. 6*B*) (current amplitude at V_h of −70 mV; scrambled shRNA-expressing astrocytes, 176 ± 46 pA, $n = 4$; *mBest1*–shRNA-expressing astrocytes, 15 ± 4 pA, $n = 5$; $^{***}p < 0.001$ vs scrambled shRNA group; unpaired *t* test) without disrupting Ca^{2+} responses by PAR-1 activation (relative change percentage of fura-2 340/380 ratio; scrambled shRNA, 100 ± 17%; *mBest1*–shRNA, 131 ± 16%; $p = 0.92$; paired *t* test). This mBest1-dependent CAAC current was also confirmed by performing whole-cell patch-clamp analysis using Ca^{2+} containing internal solution in cultured astrocytes (Fig. 6*C*) (holding current at V_h of −70 mV; scrambled shRNA-expressing astrocytes, 174 ± 7 pA, $n = 10$; *mBest1*–shRNA-expressing astrocytes, 50 ± 8 pA, $n = 11$; $^{***}p < 0.001$ vs scrambled shRNA group; unpaired *t* test). These results indicate that *mBest1* expression in astrocytes is necessary for functional CAAC, consistent with our working hypothesis that *mBest1* encodes CAAC channels.

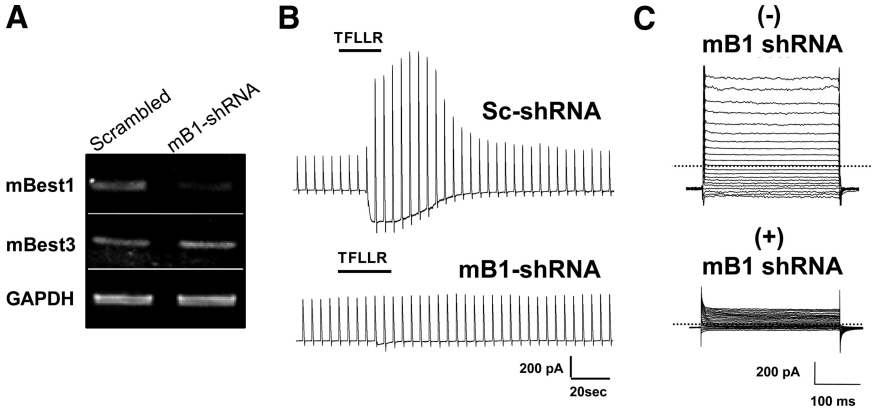

Figure 6. Best1 is a functional CAAC in cultured astrocytes. ***A***, Representative RT-PCR analysis of *mBest1*–shRNA (mB1-shRNA) in cultured astrocytes. Cells were incubated with *mBest1*–shRNA or scrambled shRNA-containing lentivirus for 72 h, and endogenous mRNA expression level of *mBest1*, *mBest3*, and *GAPDH* were subsequently analyzed. ***B***, Representative perforated-patch-current recording from scrambled shRNA (Sc-shRNA) or *mBest1*–shRNA (mB1-shRNA)-expressing cultured astrocytes. The current responses were recorded in response to a voltage ramp command (from −100 to +100 mV, 1 s duration, 0.2 Hz; V_h of −70 mV) before and after TFLLR treatment. ***C***, Representative current responses recorded with whole-cell patch clamp using 4.5 μM Ca^{2+}-containing pipette solution in response to voltage steps (from −100 to +100 mV) in astrocytes expressing enhanced green fluorescent protein or scrambled shRNA [(−) mB1 shRNA] or *mBest1*–shRNA [(+) mB1 shRNA].

mBest1 encodes CAAC current in hippocampal astrocyte

Because cultured astrocytes were shown to have different gene expression profiles than astrocytes in tissue (Cahoy et al., 2008), it is possible that our observation of mBest1-mediated CAAC in cultured astrocytes might not be representative of the *in vivo* condition. To test whether astrocytes *in situ* display the CAAC current, we first characterized Ca^{2+}-induced current from hippocampal CA1 astrocytes under whole-cell patch-clamp mode (Fig. 7*A*). SR-101, which has been used for labeling astrocytes in brain slice, was used for identifying astrocytes. To induce a Ca^{2+} increase in hippocampal CA1 astrocytes, we applied a brief pressure pulse to a TFLLR-containing micropipette (~500 μM, 1 s) that was placed near a single SR-101-loaded astrocyte. PAR-1 activation by the pulse of TFLLR induced an inward current at a holding potential of −70 mV (59 ± 17 pA; $n = 6$), which was significantly blocked by pretreatment of anion channel blocker (NPPB, 100 μM; 14 ± 5 pA; $n = 6$) or in the presence of Ca^{2+} chelator in the patch pipette solution (BAPTA, 10 mM; 9 ± 2 pA; $n = 6$) (Fig. 7*D*). It is possible that Ca^{2+}-induced astrocytic volume increase and subsequent activation of a VRAC might be responsible for this PAR-1-induced Cl^- current (Takano et al., 2005). However, the PAR-1-induced current was not affected by pretreatment of hypertonic ACSF (15% higher osmolarity than isotonic ACSF for at least 20 min; 57 ± 17 pA; $n = 3$), which argues against the possibility of PAR-1-induced VRAC activation (Fig. 7*D*). Moreover, PAR-1-induced current was not significantly changed by using Cs-containing pipette solution, suggesting that the PAR-1-induced current is minimally influenced by a Ca^{2+}-activated K conductance in our experimental condition (Cecchi et al., 1987; Hu et al., 1989) (K pipette, 59 ± 17 pA, $n = 6$; Cs pipette, 40 ± 16 pA, $n = 8$; $p = 0.12$, unpaired *t* test). These results demonstrate that PAR-1 activation leads to the generation of a CAAC current in hippocampal CA1 astrocytes in acutely prepared brain slices, the properties of which are similar to cultured astrocytes. Next, using lentiviral shRNA expression system, we expressed scrambled or *mBest1*–shRNA in hippocampal CA1 astrocytes to determine whether mBest1 mediates the channel-dependent CAAC current. Our immunohistochemical analysis showed that lentiviral expression of *mBest1*–shRNA significantly reduces the expression level of mBest1 protein in hippocampal slice (supplemental Fig. 2, available at www.jneurosci.org as supplemental material). Using this gene silencing tool, we measured CAAC current in scrambled or *mBest1*-shRNA-expressing astrocytes. Similar to the measurements in cultured astrocytes, PAR-1-induced CAAC current was significantly reduced in *mBest1*—shRNA-expressing astrocytes compared with scrambled shRNA-expressing astrocytes (Fig. 7*C*,*D*) (scrambled shRNA, 37 ± 4 pA, $n = 12$; *mBest1*–shRNA, 11 ± 4 pA, $n = 7$). Altogether, these results demonstrated that mBest1 is the functional CAAC both in *in vitro* and *in vivo* astrocytes.

Discussion

Functional expression of CAAC in astrocyte

In this study, we have demonstrated that in cultured astrocytes the activation of a GPCR such as PAR-1 can induce a Ca^{2+}-dependent current. This current was functionally similar to the previously characterized CAACs with overlapping properties, such as the rank order of anion permeability, outwardly rectifying current–voltage relationship, and the sensitivity to anion channel blockers (Figs. 1–3). This current was also observed in hippocampal CA1 astrocytes in hippocampal slices, which was similarly dependent on Ca^{2+} (Fig. 7).

Because of the complex and overlapping pharmacological targets of various anion channel blockers such as niflumic acid and NPPB (Greenwood and Leblanc, 2007), it is possible that other channels might be involved in PAR-1-induced current from cultured or hippocampal CA1 astrocytes. Our results show that activation of the gap-junction hemichannel (Ye et al., 2003) and chlorotoxin-sensitive chloride channel are unlikely to mediate CAAC because of the insensitivity of the current by the treatment of corresponding blockers (see Results). Other possible contributions by either nonselective cation channels or Ca^{2+}-activated

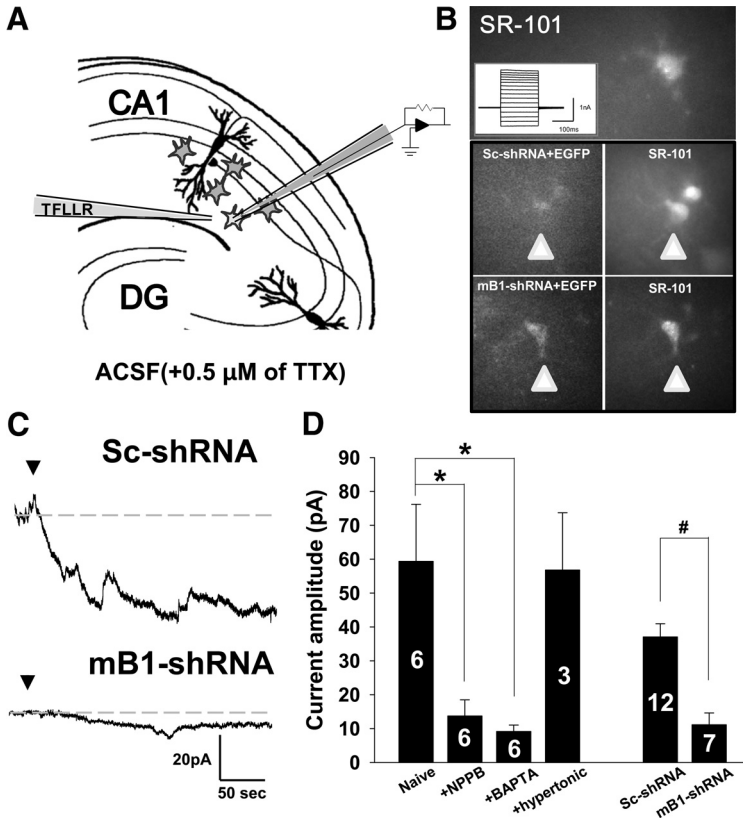

Figure 7. mBest1-mediated CAAC current from mouse hippocampal CA1 astrocytes. ***A***, Schematic diagram shows the whole-cell CAAC current measurement in CA1 astrocytes in hippocampal slices. TFLLR puff (~1 s, 500 μM) was briefly applied from a pressurized pipette. PAR-1-induced increase in $[Ca^{2+}]_i$ and a Ca^{2+}-activated current in astrocytes from hippocampal CA1 region. To minimize the effects from spontaneous activity neighboring neurons, ACSF containing 0.5 μM tetrodotoxin (TTX) was used. ***B***, Top, Representative image of SR-101-loaded astrocytes and its current response during a series of voltage steps (from −100 to +100 mV); this protocol was used to identify astrocytes in the hippocampal CA1 region. Bottom, Representative colocalization images of astrocytes expressing enhanced green fluorescent protein (EGFP) as a marker for lentiviral shRNA and SR-101 fluorescence as a marker for astrocyte. Arrowhead indicates the colocalization between enhanced green fluorescent protein and SR-101 fluorescence in the same cell from hippocampal CA1 region. ***C***, Representative current response induced by TFLLR application from scrambled shRNA (Sc-shRNA)-expressing or *mBest1*–shRNA (mB1-shRNA)-expressing astrocytes at V_h of −70 mV. The dotted line indicates baseline before TFLLR application. ***D***, Bar graph summarizes the mean current amplitude at V_h of −70 mV ± SEM (*$p <$ 0.05 vs naive astrocyte, one-way ANOVA with Dunnett's multiple comparison test; $^{\#}p < 0.05$ vs scrambled shRNA-expressing astrocyte, unpaired *t* test). Numbers of determinations are indicated on the bar graph.

K^+ conductances (Gebremedhin et al., 2003) seemed unlikely given the good agreement between the observed reversal potential and calculated E_{Cl} (Fig. 3*C*,*D*), as well as given the use of Cs^+- or TEA-containing internal solution for whole-cell patch-clamp recordings (Figs. 5, 7). Collectively, despite the caveats of using poorly selective anion channel blockers for identifying CAAC conductance, our results provide strong evidence that hippocampal astrocytes express functional CAAC. Finally, the possibility exists that a Ca^{2+}-induced volume increase and subsequent VRAC activation could contribute in part to the PAR-1-induced current we observed. However, we found that the PAR-1-induced current in hippocampal astrocytes was unchanged in hypertonic ACSF condition, indicating that the involvement of VRAC is minimal in PAR-1-induced anion conductance (Fig. 7*D*).

mBest1 encodes CAAC in astrocytes

The results from RT-PCR, single-cell PCR, *in situ* hybridization, and gene silencing experiments all indicate that the CAAC current observed in mouse brain astrocytes is mediated by the mBest1 channel. Among the previously suggested molecular candidates for CAAC, including ClC-3, CLCA, and bestrophin channels, bestrophin channel appears to be the best candidate for CAAC because the Cl^- currents from bestrophin-expressing cells showed many of the properties of native CAAC properties (Sun et al., 2002; Qu et al., 2004; Barro Soria et al., 2006), such as Ca^{2+} activation, sensitivity to niflumic acid, and outwardly rectifying current–voltage relationship (Fig. 5*A*). ClC-3 gene was excluded from the list of candidates genes, because it has been reported that ClC3-deleted mice displayed the impaired CaMKII-activated but intact Ca^{2+}-activated anion conductance (Hartzell et al., 2005). Our results showed a lack of expression of CLCA in astrocytes, and CLCA possesses properties that are inconsistent with astrocytic CAAC (Fig. 4*A*) (Eggermont, 2004). Despite their strong expression, *Ttyh1* and *Ttyh2* are insensitive to Ca^{2+} (Suzuki and Mizuno, 2004). *Ttyh3*, one of the *Ttyh* family genes showing Ca^{2+}-dependent generation of maxi-anion current when expressed heterologously in CHO cells, was also unlikely to mediate CAAC because *Ttyh3* response displays a linear current–voltage relationship and is sensitive to 4,4′-diisothiocyanatostilbene-2, 2′-disulfonic acid but not to niflumic acid (Suzuki and Mizuno, 2004). Recently, the transmembrane protein 16A and transmembrane protein 16B (TMEM16A and TMEM16B) genes were suggested as a bona fide CAAC (Caputo et al., 2008; Schroeder et al., 2008; Yang et al., 2008; Rock et al., 2009), but, because of the low expression level in brain, TMEM16A or TMEM16B seems unlikely to encode astrocytic CAAC (Schroeder et al., 2008; Yang et al., 2008).

The possible contribution of mBest3 to the CAAC current in astrocyte appears to be minimal for the following reasons. First, mBest3 transcript is expressed at much lower level than that of mBest1 in brain. Second, mBest3, which was previously called mBest4, was reported to be nonfunctional for generating anion conductance unless a portion of the C terminus is truncated (Qu et al., 2006a). Finally, CAAC current was almost completely impaired by mBest1 gene silencing in astrocytes (Figs. 6, 7). Nevertheless, we cannot exclude the possibility of a regulatory function for mBest3 in mBest1-mediated CAAC current. We also cannot exclude the existence of C-terminally truncated form of mBest3 in astrocytes. Future study should be directed to elucidate the exact role of mBest3 in astrocytes and neurons, possibly using mBest3-specific gene silencing tool. Collectively, these results strongly support the idea that Best1 channel is a functional CAAC in astrocytes.

In a recent report, it has been proposed that bestrophin can function not only as a CAAC but also as a regulator of L-type Ca^{2+} channels (Rosenthal et al., 2006; Yu et al., 2008). In astrocytes, the source of Ca^{2+} increase is mainly from intracellular Ca^{2+} stores after GPCR activation rather than from extracellular

Ca^{2+} entry through voltage-gated Ca^{2+} channels (Fig. 1). Despite the previous reports about functional expression of L-type Ca^{2+} channel in astrocytes (Latour et al., 2003; D'Ascenzo et al., 2004), we found that PAR-1 activation-induced Ca^{2+} responses were intact during the treatment astrocytes with the selective L-type Ca^{2+} channel blocker nimodipine (2 μM; $n = 3$) (data not shown). In addition, *mBest1*–shRNA expression in astrocytes did not affect the TFLLR-induced Ca^{2+} responses (see Results). Furthermore, mBest1 channels lack a functional domain for interactions with L-type Ca^{2+} channels. Therefore, at least in mouse astrocytes, it is unlikely that mBest1 acts as a Ca^{2+} channel regulator.

The present study provides compelling evidence for functional expression of CAAC in astrocytes. Our results revealed that Best1 is functionally expressed in astrocytes and encodes the channel that gives rise to most of the CAAC in astrocytes. The physiological function of astrocytic CAAC and Best1 channel remains to be explored, but the results and molecular tools described here should provide an opportunity to address many interesting questions regarding the physiological role of anion channels in astrocytes.

References

Abdullaev IF, Rudkouskaya A, Schools GP, Kimelberg HK, Mongin AA (2006) Pharmacological comparison of swelling-activated excitatory amino acid release and Cl^- currents in cultured rat astrocytes. J Physiol 572:677–689.

Barro Soria R, Spitzner M, Schreiber R, Kunzelmann K (2006) Bestrophin 1 enables Ca^{2+} activated Cl^- conductance in epithelia. J Biol Chem 282:1313–1321.

Cahoy JD, Emery B, Kaushal A, Foo LC, Zamanian JL, Christopherson KS, Xing Y, Lubischer JL, Krieg PA, Krupenko SA, Thompson WJ, Barres BA (2008) A transcriptome database for astrocytes, neurons, and oligodendrocytes: a new resource for understanding brain development and function. J Neurosci 28:264–278.

Caputo A, Caci E, Ferrera L, Pedemonte N, Barsanti C, Sondo E, Pfeffer U, Ravazzolo R, Zegarra-Moran O, Galietta LJ (2008) TMEM16A, a membrane protein associated with calcium-dependent chloride channel activity. Science 322:590–594.

Cecchi X, Wolff D, Alvarez O, Latorre R (1987) Mechanisms of Cs^+ blockade in a Ca^{2+}-activated K^+ channel from smooth muscle. Biophys J 52:707–716.

Cetin A, Komai S, Eliava M, Seeburg PH, Osten P (2006) Stereotaxic gene delivery in the rodent brain. Nat Protoc 1:3166–3173.

Chien LT, Zhang ZR, Hartzell HC (2006) Single Cl^- channels activated by Ca^{2+} in *Drosophila* S2 cells are mediated by bestrophins. J Gen Physiol 128:247–259.

Clapp LH, Turner JL, Kozlowski RZ (1996) Ca^{2+}-activated Cl^- currents in pulmonary arterial myocytes. Am J Physiol 270:H1577–H1584.

Cliff WH, Frizzell RA (1990) Separate Cl^- conductances activated by cAMP and Ca^{2+} in Cl^--secreting epithelial cells. Proc Natl Acad Sci U S A 87:4956–4960.

Crépel V, Panenka W, Kelly ME, MacVicar BA (1998) Mitogen-activated protein and tyrosine kinases in the activation of astrocyte volume-activated chloride current. J Neurosci 18:1196–1206.

Dalton S, Gerzanich V, Chen M, Dong Y, Shuba Y, Simard JM (2003) Chlorotoxin-sensitive Ca^{2+}-activated Cl^- channel in type R2 reactive astrocytes from adult rat brain. Glia 42:325–339.

d'Anglemont de Tassigny A, Souktani R, Ghaleb B, Henry P, Berdeaux A (2003) Structure and pharmacology of swelling-sensitive chloride channels, I(Cl,swell). Fundam Clin Pharmacol 17:539–553.

D'Ascenzo M, Vairano M, Andreassi C, Navarra P, Azzena GB, Grassi C (2004) Electrophysiological and molecular evidence of L- (Cav1), N- (Cav2.2), and R- (Cav2.3) type Ca^{2+} channels in rat cortical astrocytes. Glia 45:354–363.

Eggermont J (2004) Calcium-activated chloride channels: (un)known, (un)loved? Proc Am Thorac Soc 1:22–27.

Gebremedhin D, Yamaura K, Zhang C, Bylund J, Koehler RC, Harder DR (2003) Metabotropic glutamate receptor activation enhances the activities of two types of Ca^{2+}-activated K^+ channels in rat hippocampal astrocytes. J Neurosci 23:1678–1687.

Greenwood IA, Leblanc N (2007) Overlapping pharmacology of Ca^{2+}-activated Cl^- and K^+ channels. Trends Pharmacol Sci 28:1–5.

Halassa MM, Fellin T, Haydon PG (2007) The tripartite synapse: roles for gliotransmission in health and disease. Trends Mol Med 13:54–63.

Hartzell C, Putzier I, Arreola J (2005) Calcium-activated chloride channels. Annu Rev Physiol 67:719–758.

Hartzell HC, Qu Z, Yu K, Xiao Q, Chien LT (2008) Molecular physiology of bestrophins: multifunctional membrane proteins linked to best disease and other retinopathies. Physiol Rev 88:639–672.

Hougaard DM, Hansen H, Larsson LI (1997) Non-radioactive in situ hybridization for mRNA with emphasis on the use of oligodeoxynucleotide probes. Histochem Cell Biol 108:335–344.

Hu SL, Yamamoto Y, Kao CY (1989) Permeation, selectivity, and blockade of the Ca^{2+}-activated potassium channel of the guinea pig taenia coli myocyte. J Gen Physiol 94:849–862.

Kadkol SS, Gage WR, Pasternack GR (1999) In situ hybridization-theory and practice. Mol Diagn 4:169–183.

Kafitz KW, Meier SD, Stephan J, Rose CR (2008) Developmental profile and properties of sulforhodamine 101: labeled glial cells in acute brain slices of rat hippocampus. J Neurosci Methods 169:84–92.

Kimelberg HK, Macvicar BA, Sontheimer H (2006) Anion channels in astrocytes: biophysics, pharmacology, and function. Glia 54:747–757.

Kunzelmann K, Milenkovic VM, Spitzner M, Soria RB, Schreiber R (2007) Calcium-dependent chloride conductance in epithelia: is there a contribution by Bestrophin? Pflugers Arch 454:879–889.

Kuruma A, Hartzell HC (1999) Dynamics of calcium regulation of chloride currents in *Xenopus* oocytes. Am J Physiol 276:C161–C175.

Kyrozis A, Reichling DB (1995) Perforated-patch recording with gramicidin avoids artifactual changes in intracellular chloride concentration. J Neurosci Methods 57:27–35.

Lambert S, Oberwinkler J (2005) Characterization of a proton-activated, outwardly rectifying anion channel. J Physiol 567:191–213.

Latour I, Hamid J, Beedle AM, Zamponi GW, Macvicar BA (2003) Expression of voltage-gated Ca^{2+} channel subtypes in cultured astrocytes. Glia 41:347–353.

Lee CJ, Mannaioni G, Yuan H, Woo DH, Gingrich MB, Traynelis SF (2007) Astrocytic control of synaptic NMDA receptors. J Physiol 581:1057–1081.

Marmorstein AD, Marmorstein LY, Rayborn M, Wang X, Hollyfield JG, Petrukhin K (2000) Bestrophin, the product of the Best vitelliform macular dystrophy gene (VMD2), localizes to the basolateral plasma membrane of the retinal pigment epithelium. Proc Natl Acad Sci U S A 97:12758–12763.

O'Driscoll KE, Leblanc N, Hatton WJ, Britton FC (2009) Functional properties of murine bestrophin 1 channel. Biochem Biophys Res Commun 384:476–481.

Parkerson KA, Sontheimer H (2004) Biophysical and pharmacological characterization of hypotonically activated chloride currents in cortical astrocytes. Glia 46:419–436.

Pifferi S, Pascarella G, Boccaccio A, Mazzatenta A, Gustincich S, Menini A, Zucchelli S (2006) Bestrophin-2 is a candidate calcium-activated chloride channel involved in olfactory transduction. Proc Natl Acad Sci U S A 103:12929–12934.

Porter JT, McCarthy KD (1997) Astrocytic neurotransmitter receptors in situ and in vivo. Prog Neurobiol 51:439–455.

Qu Z, Hartzell HC (2001) Functional geometry of the permeation pathway of Ca^{2+}-activated Cl^- channels inferred from analysis of voltage-dependent block. J Biol Chem 276:18423–18429.

Qu Z, Hartzell C (2004) Determinants of anion permeation in the second transmembrane domain of the mouse bestrophin-2 chloride channel. J Gen Physiol 124:371–382.

Qu Z, Wei RW, Mann W, Hartzell HC (2003) Two bestrophins cloned from *Xenopus laevis* oocytes express Ca^{2+}-activated Cl^- currents. J Biol Chem 278:49563–49572.

Qu Z, Fischmeister R, Hartzell C (2004) Mouse bestrophin-2 is a bona fide Cl^- channel: identification of a residue important in anion binding and conduction. J Gen Physiol 123:327–340.

Qu Z, Cui Y, Hartzell C (2006a) A short motif in the C-terminus of mouse bestrophin 3 [corrected] inhibits its activation as a Cl channel. FEBS Lett 580:2141–2146.

Qu Z, Chien LT, Cui Y, Hartzell HC (2006b) The anion-selective pore of the

bestrophins, a family of chloride channels associated with retinal degeneration. J Neurosci 26:5411–5419.

Ramos-Mandujano G, Vázquez-Juárez E, Hernández-Benítez R, Pasantes-Morales H (2007) Thrombin potently enhances swelling-sensitive glutamate efflux from cultured astrocytes. Glia 55:917–925.

Rock JR, O'Neal WK, Gabriel SE, Randell SH, Harfe BD, Boucher RC, Grubb BR (2009) Transmembrane protein 16A (TMEM16A) is a Ca^{2+}-regulated Cl^- secretory channel in mouse airways. J Biol Chem 284:14875–14880.

Rosenthal R, Bakall B, Kinnick T, Peachey N, Wimmers S, Wadelius C, Marmorstein A, Strauss O (2006) Expression of bestrophin-1, the product of the VMD2 gene, modulates voltage-dependent Ca^{2+} channels in retinal pigment epithelial cells. FASEB J 20:178–180.

Schroeder BC, Cheng T, Jan YN, Jan LY (2008) Expression cloning of TMEM16A as a calcium-activated chloride channel subunit. Cell 134:1019–1029.

Scott RH, Sutton KG, Griffin A, Stapleton SR, Currie KP (1995) Aspects of calcium-activated chloride currents: a neuronal perspective. Pharmacol Ther 66:535–565.

Sun H, Tsunenari T, Yau KW, Nathans J (2002) The vitelliform macular dystrophy protein defines a new family of chloride channels. Proc Natl Acad Sci U S A 99:4008–4013.

Suzuki M, Mizuno A (2004) A novel human Cl^- channel family related to *Drosophila* flightless locus. J Biol Chem 279:22461–22468.

Takano T, Kang J, Jaiswal JK, Simon SM, Lin JH, Yu Y, Li Y, Yang J, Dienel G, Zielke HR, Nedergaard M (2005) Receptor-mediated glutamate release from volume sensitive channels in astrocytes. Proc Natl Acad Sci U S A 102:16466–16471.

Ventura A, Meissner A, Dillon CP, McManus M, Sharp PA, Van Parijs L, Jaenisch R, Jacks T (2004) Cre-lox-regulated conditional RNA interference from transgenes. Proc Natl Acad Sci U S A 101:10380–10385.

Volterra A, Meldolesi J (2005) Astrocytes, from brain glue to communication elements: the revolution continues. Nat Rev Neurosci 6:626–640.

Walz W (2002) Chloride/anion channels in glial cell membranes. Glia 40:1–10.

Yang YD, Cho H, Koo JY, Tak MH, Cho Y, Shim WS, Park SP, Lee J, Lee B, Kim BM, Raouf R, Shin YK, Oh U (2008) TMEM16A confers receptor-activated calcium-dependent chloride conductance. Nature 455:1210–1215.

Ye ZC, Wyeth MS, Baltan-Tekkok S, Ransom BR (2003) Functional hemichannels in astrocytes: a novel mechanism of glutamate release. J Neurosci 23:3588–3596.

Yu K, Xiao Q, Cui G, Lee A, Hartzell HC (2008) The best disease-linked Cl^- channel hBest1 regulates Ca_V1 (L-type) Ca^{2+} channels via Src-homology-binding domains. J Neurosci 28:5660–5670.